The Journal of Chemical Physics

RESEARCH ARTICLE | FEBRUARY 02 2023

Micro-/macroscopic and density functional studies of the interactions between molybdenum trioxide and C_{60} molecule

Masato Nakaya ; Takuya Kawai; Shinta Watanabe ; Jun Onoe

J. Chem. Phys. 158, 054701 (2023)
https://doi.org/10.1063/5.0134207

The Journal of Chemical Physics ARTICLE scitation.org/journal/jcp

Micro-/macroscopic and density functional studies of the interactions between molybdenum trioxide and C_{60} molecule

Cite as: J. Chem. Phys. 158, 054701 (2023); doi: 10.1063/5.0134207
Submitted: 9 November 2022 • Accepted: 16 January 2023 •
Published Online: 2 February 2023

Masato Nakaya, Takuya Kawai, Shinta Watanabe, and Jun Onoe[a]

AFFILIATIONS

Department of Energy Science and Engineering, Nagoya University, Furo-cho, Chikusa-ku, Nagoya 464-8603, Japan

[a]Author to whom correspondence should be addressed: j-onoe@energy.nagoya-u.ac.jp. Tel./Fax: +81-52-789-3784

ABSTRACT

We have investigated the interactions between C_{60} and $(MoO_3)_n$ using scanning tunneling microscopy with spectroscopy (STM/STS) and *ex situ* ultraviolet–visible–near-infrared (UV–vis–NIR) spectroscopy in combination with density functional theory (DFT) calculations. The formation of $(MoO_3)_n$ chemically bound to C_{60} is energetically favorable due to $\Delta G < 0$ for n = 1, 2, 4, 6, 8, and 9, and they well reproduced the histogram of the height of $(MoO_3)_n$ on the C_{60} (111) terrace obtained by a STM height-profile. STS results demonstrated the upward energy shift of both highest occupied molecular orbital (HOMO) and lowest unoccupied molecular orbital (LUMO) of C_{60} in the vicinity of $(MoO_3)_n$ (n = 6 or 9), which is consistent with the previous results of the co-deposited C_{60}/MoO_3 film obtained using photoemission and inverse photoemission spectroscopy [Wang and Gao, Appl. Phys. Lett. **105**, 111601 (2014), Yang *et al.*, J. Phys.: Condens. Matter **28**, 185502 (2016), and Li *et al.*, J. Phys. Chem. C **118**, 4869 (2014)]. Theoretical calculations of $(MoO_3)_n$ (n = 1, 2, 4, 6, 8, and 9) chemically bound to C_{60} indicated that 0.01–0.32 holes are injected into C_{60} by $(MoO_3)_n$ nanoclusters, and UV–vis–NIR and DFT results found that the hole doping to C_{60} is caused via the electron transfer from the HOMO of C_{60} to the LUMO of $(MoO_3)_n$. Furthermore, it is noted that the C_{60}–$(MoO_3)_n$ interactions exhibit a high heat resistance up to 250 °C by examining the UV–vis–NIR spectra of a co-deposited C_{60}/MoO_3 (6:4) film before and after thermal annealing. The present findings provide useful information for the practical use of P-type C_{60}-based thermoelectric devices.

I. INTRODUCTION

Fullerene C_{60}[1] has been well known to be investigated fundamentally and industrially so far.[2,3] Recently, the C_{60} film has been reported to exhibit a giant Seebeck coefficient (S) of more than 150 mV K^{-1} (27 °C)[4] and a lower thermal conductivity (κ) of 0.4 Wm^{-1} K^{-1} (27 °C)[5] when compared to those (S = 0.27 mV K^{-1}, κ = 1.6 Wm^{-1} K^{-1} at 27 °C) of Bi_2Te_3[6] used practically, thus being expected to be one of the powerful candidates for next-generation thermoelectric devices.

However, to realize the C_{60}-based thermoelectric devices, there are two important issues to be solved for practical use. One is that the electrical conductivity ($\sigma = 10^{-5}$ Ω^{-1} cm^{-1}) of C_{60} films[7] is much smaller by 10^{-7} order than that (σ = 307 Ω^{-1} cm^{-1}) of Bi_2Te_3.[6] To increase the figure of merit ($Z = S^2\sigma/\kappa$) used as a performance index for thermoelectric materials, it is necessary to increase the σ of C_{60} films drastically while suppressing the decrease in the S, because there is a trade-off relationship between S and σ derived from Mott's formula.[8] For example, a typical way to increase the σ of C_{60} films is to use dopants, such as alkali metals (potassium: K)[7,9] and organic–dimetal complexes,[10] in the films. However, while the σ was increased with a fraction of K in the film, the S correspondingly decreased according to Mott's formula.[8] One possible way to break the S–σ trade-off relationship is to employ C_{60} photopolymerization,[11] because a part of polymerization in C_{60} films contributes to increasing the σ while suppressing the decrease in the S, which implies that a perfect C_{60} polymer network via [2 + 2] four-membered ring is randomly broken to suppress phonon-mediated thermal conductivity. This idea is quite similar to that of the carrier energy filtering effects.[12,13]

The other issue is that P-type C_{60}-based thermoelectric materials are harder to be produced than N-type ones, because the

C_{60} molecule has a high ionization potential (I_p) of 6.4 eV against the vacuum level (VL).[14,15] This issue also becomes a high barrier against the realization of not only thermoelectric devices but also field-effect transistors (FETs), light-emitting diodes (LEDs), organic photovoltaic cells (OPVs), etc., based on C_{60}. One candidate of hole dopant for C_{60} films is MoO_3 because of a high electron affinity (E_A) of 6.7 eV against VL.[16] Indeed, MoO_3-doped C_{60} films were reported to work as a P-type component of P-channel FET[17] and homojunction OPV,[15] although the doping efficiency (~3%)[18] and the hole mobility ($1.52–5.61 \times 10^{-3}$ cm^2 V^{-1} s^{-1})[17] were both considerably very small.

The previous studies[19,20] found from the photoelectron spectra of MoO_3/C_{60} co-deposited films that the highest occupied molecular orbital (HOMO) and the lowest unoccupied molecular orbital (LUMO) bands of C_{60} films were simultaneously shifted to a lower binding energy with an increasing amount of MoO_3 doped to the C_{60} film. For example, the energy difference between the HOMO onset and E_F decreased from 1.79 eV (MoO_3: 0 wt. %) to less than 0.3 eV (MoO_3: 85 wt. %), indicating the formation of p-type films.[20] This energy shift was attributed to the electron transfer from the HOMO of C_{60} to MoO_3. For the thermal evaporation of MoO_3 powder in vacuum, Berkowitz and Inghram performed mass spectrometric analysis of the vapor in thermodynamic equilibrium with powdered MoO_3 mounted in a Knudsen cell and have shown that the vapor phase consists predominantly of $(MoO_3)_3$, $(MoO_3)_4$, and $(MoO_3)_5$ clusters.[21] Accordingly, it is necessary to perform microscopic measurements in order to understand the interactions between C_{60} and individual $(MoO_3)_n$ nanoclusters more precisely, which provides an insight into the fabrication of p-type C_{60}-based thermoelectric devices.

In the present study, we have investigated the interactions between C_{60} and $(MoO_3)_n$ using *in situ* ultrahigh vacuum (UHV) scanning tunneling microscopy with spectroscopy (STM/STS) and *ex situ* ultraviolet–visible–near-infrared (UV–vis–NIR) spectroscopy in combination with first-principles calculations based on density functional theory.

II. EXPERIMENTS AND THEORETICAL CALCULATIONS

STM/STS measurements were performed in a UHV apparatus equipped with a preparation chamber (base pressure: 7.0×10^{-8} Pa) and an analysis chamber (base pressure: 2.0×10^{-8} Pa) that are separated from each other via a gate valve. An ultrathin C_{60} film with a few layers (2–3 layers) was formed by the following procedures. First, the Si(111)7 × 7 surface was prepared by repeated flash annealing of the Si(111) substrate (N-type, σ = 40–67 Ω^{-1} cm^{-1}) at 1220 °C for 6 s in the preparation chamber. Subsequently, the Si(111)$\sqrt{3} \times \sqrt{3}$R30°-Ag [referred to as Si(111)$\sqrt{3}$-Ag] surface was prepared by depositing 1 monolayer (ML) (7.83×10^{14} atoms/cm^2) of Ag atoms on the Si(111)7 × 7 surface at 600 °C.[22] The reason behind the use of the Si(111)$\sqrt{3}$-Ag substrate is the high stability with the inert surface, resulting in van der Waals interactions with C_{60} molecules comparable to that in a solid C_{60}.[22] In order to form an ultrathin C_{60} film, C_{60} molecules were deposited on the Si(111)$\sqrt{3}$-Ag surface at room temperature (RT) by the thermal evaporation of C_{60} powder (99.95% in purity) mounted in a quartz crucible maintaining a deposition rate of 0.15 nm/min. Then, $(MoO_3)_n$ nanoclusters were deposited on the C_{60} ultrathin film at RT by the thermal evaporation of powdered MoO_3 (99.9% in purity) mounted in an alumina crucible maintaining a deposition rate of 0.06 nm/min. Thereafter, $(MoO_3)_n$ deposited on the C_{60} ultrathin film was transferred to the analysis UHV chamber via a magnet feedthrough and measured by STM/STS (Omicron STM1) at RT. We used electrochemically etched Pt–20%Ir tips after the thermal cleaning of the tip apex in the UHV chamber for STM/STS measurements. The STM/STS data thus obtained were analyzed using WSxM.46.[23]

A C_{60}/MoO_3 composite film was formed by the co-deposition of C_{60} and MoO_3 molecules at RT on a quartz substrate in a UHV chamber (base pressure: 1.0×10^{-6} Pa) for UV–vis–NIR measurements. The quartz substrate was cleaned by thermal annealing at 200 °C for 5 h in the UHV chamber prior to co-deposition. The deposition rate of C_{60} and MoO_3 molecules was set to 2.1 and 0.7 nm/min, respectively. The C_{60}/MoO_3 composite film thus formed was measured using UV–Vis–NIR spectroscopy (JASCO V-630) at RT in air.

First-principles calculations were performed using Gaussian09[24] based on density functional theory (DFT).[25,26] The structure of individual C_{60}–$(MoO_3)_n$ (n = 1–9) heterodimers was geometrically optimized using the def2-TZVP basis set[27] and CAM-B3LYP exchange-correlation functional.[28] Here, the core electrons of Mo were considered as an effective core potential in all calculations[29] and the basis set used in the present study was taken from the "Basis Set Exchange Library."[30] In addition, the long-range electron correlations due to van der Waals interactions were taken into account by the DFT–D3 method.[31] To reveal the bond characters between C_{60} and $(MoO_3)_n$ (n = 1–9) heterodimers, we examined the localized orbital locator (LOL)[32] using Multiwfn program.[33] Furthermore, the neutral singlet state was calculated for the entire system. The same results were obtained for both the spin polarized and spin non-polarized states. A change in the free Gibbs energy (ΔG) for the heterodimer formation was estimated by frequency calculations of the optimized structures at 298.15 K under 0.1 MPa. The theoretical UV–vis–NIR absorption spectra of C_{60}–$(MoO_3)_n$ heterodimers were calculated by the time-dependent DFT (TD-DFT) method.[34] In these calculations, 400 singlet states were considered as one-electron excitation states. The calculated oscillator strength was expressed using the Gaussian function with a full-width-at-half-maximum of 0.15 eV. The amount of effective charges on C_{60} and $(MoO_3)_n$ was obtained using Natural Bond Orbital (NBO) analysis.[35]

III. RESULTS AND DISCUSSION

Figure 1(a) shows the STM images of the second- and third-layer terraces (left) and the high-resolution STM image of the third layer (right) for the ultrathin C_{60} film. The hexagonal arrangement with an intermolecular distance of 1.0 nm was observed, which is in good agreement with the arrangement of the (111) surface of the face-centered cubic (fcc) C_{60} bulk crystal.[36] This indicates that the van der Waals interaction between the Si(111)$\sqrt{3}$-Ag surface and C_{60} molecules results in the formation of the close-packed hexagonal arrangements.[22] Figure 1(b) shows the STM image of the C_{60} film after MoO_3 deposition for 1 min (left), where some large bright spots marked by violet dotted circles were observed on the terrace, step edge, and domain boundary. Since the number of spots increased with the deposition time of MoO_3 on a C_{60} monolayer (Fig. S1),

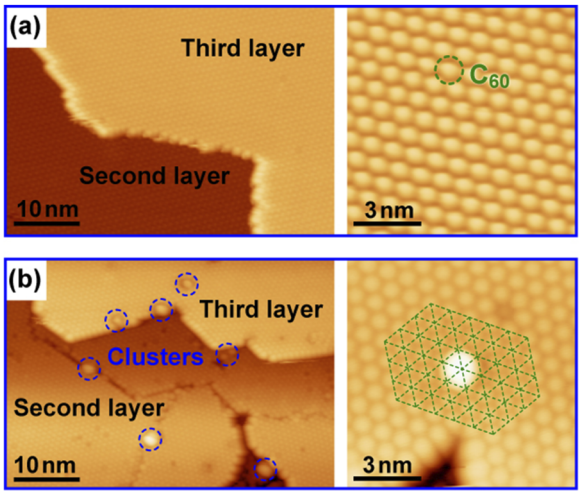

FIG. 1. STM images of ultrathin C_{60} films (a) before and (b) after the MoO_3 deposition. Left and right images in (a) and (b) were measured in the ranges of 50 × 35 nm^2 and 10 × 10 nm^2, respectively. All STM images were observed at V_s = 2.0 V and I_t = 20 pA.

these spots can be assigned to $(MoO_3)_n$ nanoclusters formed on the C_{60} surface. Figure 1(b) (right) shows the high-resolution STM image of a single $(MoO_3)_n$ nanocluster formed on the C_{60} third-layer terrace. Here, individual intersections of the superimposed triangular mesh (green dotted lines) correspond to the center position of individual C_{60} molecules. This indicates that the center of the nanocluster was located on the mesh intersection. Since the other nanoclusters formed on any terrace showed similar results, the $(MoO_3)_n$ nanoclusters are adsorbed on the top site of the C_{60}(111) surface. Since it is difficult to determine the adsorption site of the nanoclusters formed on the step edge or domain boundary accurately from the STM images, we focus on the $(MoO_3)_n$ nanoclusters formed on the terraces of the C_{60} ultrathin film.

Figure 2(a) shows the histogram of the height (h_c) of 200 $(MoO_3)_n$ nanoclusters formed on the terrace by measuring STM-height profiles at a sample bias (V_s) of 2.0 V and at a tunneling current (I_t) of 20 pA. The histogram shows a broad distribution with a peak top of h_c = 0.4–0.6 nm. Li *et al.* investigated the Infrared Reflection Absorption Spectroscopy (IRAS) spectra of thermally evaporated MoO_3 clusters suspended in a Kr matrix by comparison with the theoretical spectra of various types of $(MoO_3)_n$ nanoclusters and obtained that 61% of $(MoO_3)_3$, 17% of $(MoO_3)_4$, 15% of $(MoO_3)_5$, and 7% of $(MoO_3)_6$ were formed in gas phase,[37] which is basically consistent with the mass spectrometric results reported previously.[21] In addition, the other smaller species, such as MoO_3 and $(MoO_3)_2$, were formed via decomposition of $(MoO_3)_n$ (n = 3–6) on surfaces.[38] These previous results strongly support that various $(MoO_3)_n$ nanoclusters were formed on the C_{60} (111) terrace by decomposition and aggregation of $(MoO_3)_n$. For oxygen-deficient MoO_{3-x} species, Kröger *et al.* examined the photoemission and inverse photoemission spectra of an evaporated MoO_3 film.[39] Since the photoemission from Mo 4d orbitals of the species was absent within the gap, they concluded that the MoO_3 film is fully oxidized. In a similar manner, we observed no density-of-states (DOS) within the gap between Hc and Lc in the STS of $(MoO_3)_n$ nanoclusters [top of Fig. 3(b)], which suggests that the MoO_{3-x} species can be excluded in the present study.

To estimate the size of $(MoO_3)_n$ nanoclusters, we theoretically examined the structure and ΔG of $(MoO_3)_n$ (n = 1–9) on the top-site of C_{60} and compared the h_c with that in the histogram shown in Fig. 2(a). Figures 2(b)–2(d) show the schematic representation of the optimized structure of individual C_{60} – $(MoO_3)_n$ (n = 1–9), the theoretical h_c with respect to n, and the ΔG of $(MoO_3)_n$ (n = 1–9) chemically bound to the top-site of C_{60} [C_{60} + $(MoO_3)_n$ → C_{60} – $(MoO_3)_n$], respectively. Here, to obtain the most stable structure of C_{60}–$(MoO_3)_n$ heterodimers, several conformations were calculated and the most stable one was selected among them [for example, the most stable C_{60}–$(MoO_3)_3$ and C_{60}–$(MoO_3)_6$ heterodimers were obtained from the results of Fig. S3]. As shown in Fig. 2(d), since the formation of C_{60}–$(MoO_3)_n$ (n = 3, 5, 7) is hard to proceed energetically because of their large positive values of ΔG, they can be excluded. Figure 2(c) shows that the theoretical h_c of $(MoO_3)_n$ on the top-site of C_{60} was estimated to be 0.27 nm (n = 1), 0.4 nm (n = 2), 0.54 nm (n = 4), 0.71 nm (n = 6), 0.83 nm (n = 8), and 0.65 nm (n = 9). These values well reproduce the histogram: the intense peaks appear in the range of 0.4–0.6 nm and the shoulder peaks appear in the range both of 0.2–0.4 nm and of 0.7–0.8 nm [Fig. 2(a)].

We next examined the electronic interactions between C_{60} and $(MoO_3)_n$ (n = 1, 2, 4, 6, 8, 9). Figure 3(a) shows the high-resolution STM image (left) and the STM-height profile (right) of a single $(MoO_3)_n$ nanocluster formed on the C_{60} third layer terrace. The h_c of the nanocluster was 0.69 nm, which is close to the theoretical h_c of $(MoO_3)_6$ (0.71 nm) or $(MoO_3)_9$ (0.65 nm) on the tope-site of C_{60} [Fig. 2(c)]. Figure 3(b) shows the STS spectra of $(MoO_3)_n$ (red), C_{60} far from $(MoO_3)_n$ (green), and C_{60} in the vicinity of $(MoO_3)_n$ (blue) corresponding to the left side STM image of Fig. 3(a), respectively. Here, the STS spectra were obtained using the current imaging tunneling spectroscopy (CITS) method[40] at the set points of I_t = 100 pA and V_s = 1.7 V and the normalized dI/dV in the region of V_s < 0 and V_s > 0 corresponds to the local DOS (LDOS) in the occupied and unoccupied states, respectively. As shown in the top of Fig. 3(b), the two peaks indicated by Hc and Lc appear in the occupied (V_s = −2.3 V) and unoccupied (V_s = +1.5 V) states, respectively. As shown in Fig. S2(b), the energy gap (3.24 eV) between H_C and L_C agrees reasonably with the theoretical HOMO–LUMO gap of $(MoO_3)_6$ (3.61 eV) or $(MoO_3)_9$ (2.92 eV) on the top-site of C_{60}, whereas Fig. S4(b) shows that the Hc–Lc energy gap is considerably smaller than that of pristine $(MoO_3)_6$ (6.93 eV) or $(MoO_3)_9$ (4.11 eV). Consequently, these results allow us to conclude that the nanocluster shown in Fig. 3(a) can be assigned to $(MoO_3)_6$ or $(MoO_3)_9$ chemically bound to C_{60} molecule.

We next discuss the impact of $(MoO_3)_n$ (n = 6 or 9) deposition on the electronic structure of C_{60} layers. In the case of C_{60} molecules far from the nanocluster [middle of Fig. 3(b), green], one peak (H_{C60}) appears at V_s = −2.6 V, whereas the other peak (L_{C60}) appears at V_s = 1.3 V. Since the intensity ratio of H_{C60}/L_{C60} (1.52) agrees well with the DOS ratio (1.67) [(the fivefold degenerate HOMO)/(the threefold degenerate LUMO)] for the pristine C_{60} molecule, the H_{C60} and L_{C60} peaks correspond to the HOMO and the LUMO, respectively. In addition, the energy difference between L_{C60} (LUMO) and the Fermi level (E_F, V_s = 0) is smaller than that between H_{C60} (HOMO) and E_F, which is well known to be

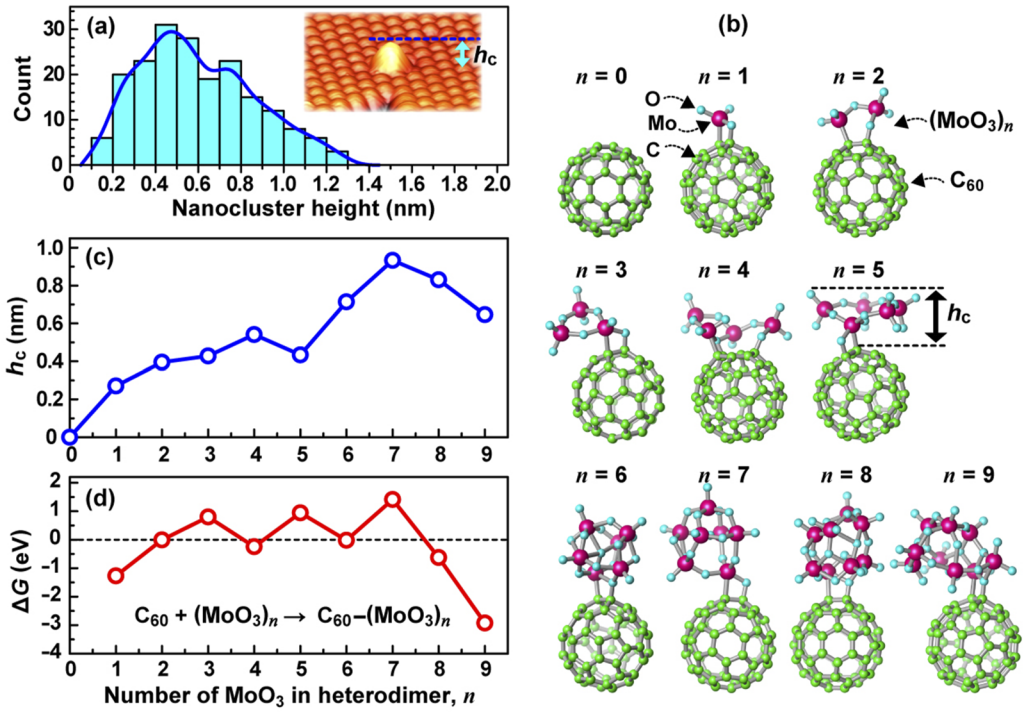

FIG. 2. (a) Histogram of the height (h_c) of each $(MoO_3)_n$ cluster. The h_c was measured by STM-height profiles at V_s = 2.2 V and I_t = 20 pA. (b) Optimized geometric structure of C_{60}–$(MoO_3)_n$ (n = 1–9) heterodimers. (c) Theoretical h_c of C_{60}–$(MoO_3)_n$ (n = 1–9) heterodimers as a function of n. (d) Gibbs free energy (ΔG) of C_{60}–$(MoO_3)_n$ heterodimers with respect to the number n.

observed for the N-type electronic and electrical properties of pristine C_{60} films.[15,17,19] On the other hand, the HOMO and LUMO energies of the C_{60} molecules in the vicinity of $(MoO_3)_n$ (n = 6 or 9) (blue) were both shifted to a higher energy (larger V_s) region by 0.15 and 0.16 eV, respectively. This suggests that the energy band of the C_{60} molecules was locally upward bended at the $C_{60}/(MoO_3)_n$ (n = 6 or 9) interface. Correspondingly, as shown in Fig. 3(c), the high-resolution STM images measured at V_s = −2.0 V (left) and 1.0 V (right) for the C_{60} molecules in the vicinity of the $(MoO_3)_n$ (n = 6 or 9) nanocluster exhibit bright and dark STM images, respectively. Since the image contrast obtained at V_s = −2.0 and 1.0 V depends on the LDOS in the tail of the HOMO and LUMO bands [indicated by red dashed lines in Fig. 3(b)], respectively, the bright (V_s = −2.0 V) and dark (V_s = 1.0 V) images were obtained by the higher energy shift in both HOMO and LUMO of C_{60} in the vicinity of the nanocluster, respectively. In other words, the change in brightness of the STM image reflected the influence of LDOS via the electron transfer from C_{60} to $(MoO_3)_n$ (n = 6 or 9). Figure 3(d) schematically illustrates the energy diagram of C_{60} molecules far from (i) and near to (ii) $(MoO_3)_n$ (n = 6 or 9) upon STS measurements. In a similar manner, the contrast of the bias-dependent STM image, bright (occupied states) and dark (unoccupied states), was observed for the acceptor and donor impurity atoms in P- and N-type semiconductor surfaces, respectively.[41,42] Namely, the N-type electronic structure of pristine C_{60} films changed to the P-type one by hole doping.[19,20] Accordingly, the upward energy shift of both HOMO and LUMO of C_{60} molecules [Fig. 3(b)] is due to the hole injection into the C_{60} molecule by $(MoO_3)_n$ (n = 6 or 9).

We also examined the bond characteristics between C_{60} and $(MoO_3)_n$ (n = 1–9) using the localized orbital locator (LOL)[32] that evaluates the electron distribution along the bonding. Figure S5(b) shows the LOL value for the bonding region of the four-membered ring [indicated by yellow in FIG. S5(a)] consisting of C–O, C–C, C–Mo, and Mo–O bonds between C_{60} and $(MoO_3)_n$ in heterodimers. As shown in Fig. S5(b), the C–C bond shows a large LOL value of 0.8, which indicates that the C–C bond in the four-membered ring exhibits a strong covalent character. In a similar manner, the C–O bond between C_{60} and $(MoO_3)_n$ also has a strong covalent character. On the other hand, the Mo–C bond has an electron distribution biased on the C atom. This indicates that the Mo–C bond has an ionic bonding character rather than a covalent one.

To estimate how much holes are doped to C_{60} by $(MoO_3)_n$, we theoretically examined the amount of charge transfer (CT) from C_{60} to $(MoO_3)_n$ (n = 1–9). Figure 3(e) shows that 0.01–0.32 electrons were transferred from a single C_{60} to a single $(MoO_3)_n$ (namely, 0.01–0.32 holes injected into C_{60}). In addition, the amount of hole injection generally tends to increase with the size of $(MoO_3)_n$ except for n = 3, 5, and 7 [$\Delta G > 0$, Fig. 2(d)]. Since Fig. S2(a) shows that the HOMO and LUMO wave functions are localized at C_{60} and $(MoO_3)_n$ ($n > 2$), respectively, the electron transfer is considered to take place between the HOMO of C_{60} and the LUMO of $(MoO_3)_n$

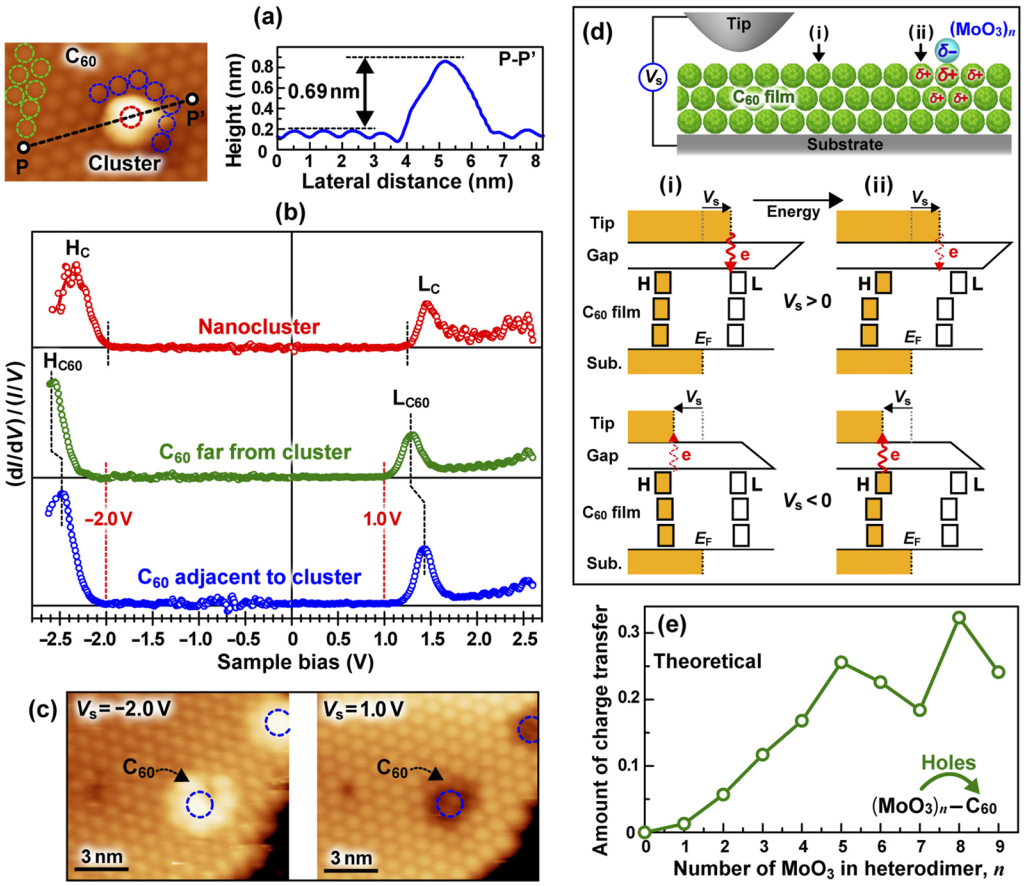

FIG. 3. (a) High-resolution STM image (left) and cross-sectional height profile (right) along P–P′ for a single $(MoO_3)_n$ nanocluster. (b) STS spectra of a single $(MoO_3)_n$ nanocluster (red) and C_{60} molecules far from (green) and in the vicinity of (blue) the nanocluster on the C_{60} third layer. Individual (d*I*/d*V*)/(*I*/*V*) data were numerically calculated from the corresponding *I*–*V* curves obtained by 100 times accumulation. The *I*–*V* measurement conditions were set to I_t = 100 pA and V_s = 1.7 V. (c) STM images of a $(MoO_3)_n$ nanocluster observed at the V_s of −2.0 V (left) and 1.0 V (right). (d) Schematic energy diagram of STS measurements for (i) pristine and (ii) hole-doped C_{60} molecules in the C_{60} third layer, where the unoccupied-states (top: V_s > 0 V) and the occupied-states (bottom: V_s < 0 V) are indicated. (e) The amount of positive effective charges on C_{60} for C_{60}–$(MoO_3)_n$ (*n* = 1–9) heterodimers.

(*n* > 2). To confirm this, we next examined the UV–vis–NIR spectra of C_{60}/(MoO_3) composite films.

Figure 4(a) shows the UV–vis–NIR spectra of a 100 nm-thick pristine C_{60} film (green), 30 nm-thick pristine MoO_3 film (blue), and 130 nm-thick C_{60}/MoO_3 composite film (red) with a (MoO_3/C_{60}) ratio of 4.6. Here, the four absorption peaks (1, 2, 3, and 5) of the pristine C_{60} film were already assigned to the intramolecular electronic transitions of (HOMO − 2/HOMO − 1 → LUMO + 2), (HOMO → LUMO + 3), (HOMO − 2/HOMO − 1 → LUMO), and (HOMO → LUMO), respectively,[43,44] whereas the broad absorption band (peak 4) originates from intermolecular electronic transitions.[45] When the C_{60} molecules were bound to $(MoO_3)_n$, the intensity of only peak 2 (HOMO → LUMO + 3) drastically decreased when compared to that of the other peaks. This strongly suggests the hole doping to the HOMO of C_{60} via the CT from C_{60} to MoO_3, because the intensity of peak 2 depends on the DOS of the HOMO.

We next discuss the origins of the wide and weak absorption band 6 newly appearing in the range of 670–1050 nm for the C_{60}/MoO_3 composite film. Figure 4(b) shows the theoretical spectra in the region of 600–1100 nm for the C_{60}–$(MoO_3)_n$ (n = 6, 8) heterodimers and indicates weak absorption peaks, denoted as a, b, and c, appearing at 651 nm for *n* = 6, 742 nm for *n* = 8, and 939 nm for *n* = 6, respectively, whereas Fig. 4(c) shows no absorption peaks theoretically obtained for pristine C_{60} and $(MoO_3)_n$ (*n* = 6, 8) nanoclusters. Theoretical analyses assigned peak a, b, and c to [C_{60}/HOMO-2 → $(MoO_3)_n$/LUMO], [C_{60}/HOMO → $(MoO_3)_n$/LUMO], and [C_{60}/HOMO → $(MoO_3)_n$/LUMO], respectively. Because of a small amount of CT between them, the intensity of individual peaks a–c will be weak. Since the intensity and wavelength of the absorption peaks depend on the cluster size *n*, the wide and weak absorption band 6 is attributed to a variety of interactions between C_{60} and $(MoO_3)_n$ clusters in the composite film.

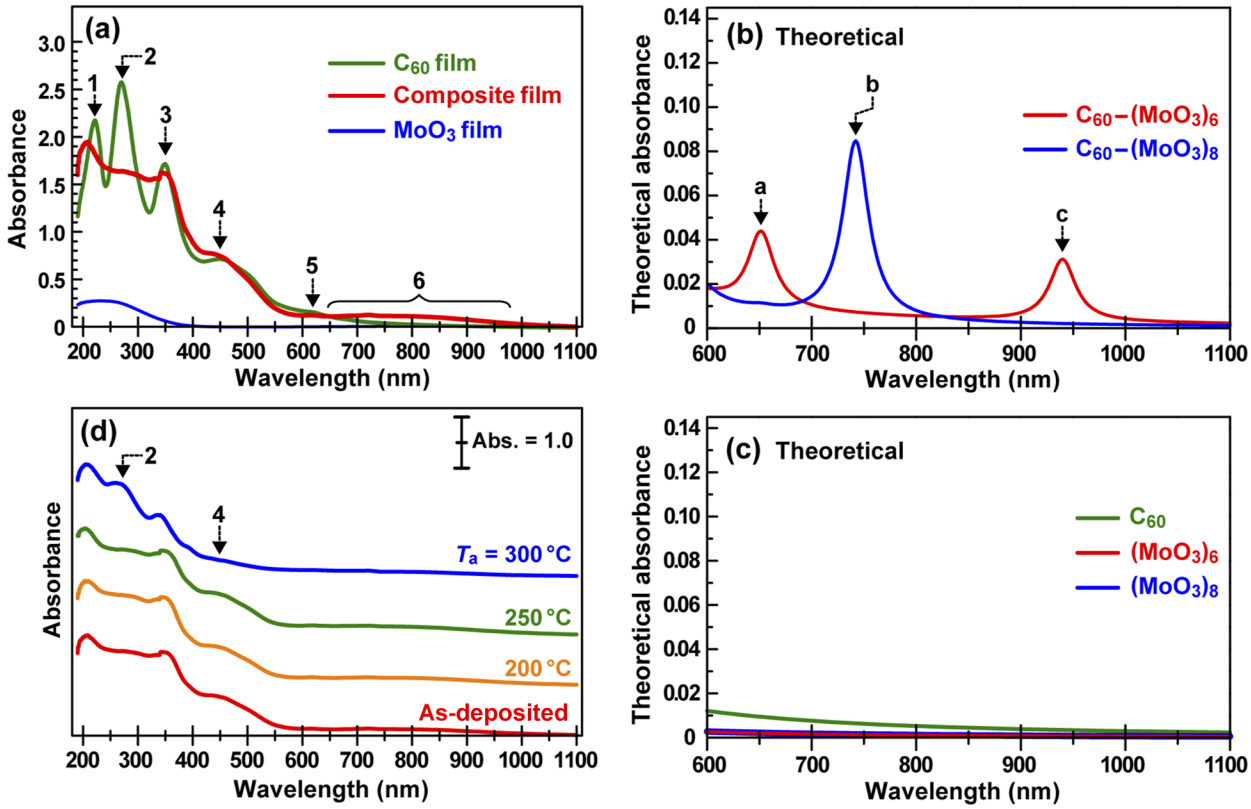

FIG. 4. (a) UV–vis–NIR spectra (λ = 190–1100 nm) of 100 nm-thick pristine C_{60} (green), 30 nm-thick pristine MoO_3 (blue), and 130 nm-thick MoO_3/C_{60} composite (red) films. (b) Theoretical absorption spectra (λ = 600–1100 nm) of C_{60}–$(MoO_3)_n$ (n = 6, 8) heterodimers. (c) Theoretical absorption spectra (λ = 600–1100 nm) of the pristine C_{60} molecule and $(MoO_3)_n$ (n = 6, 8) nanoclusters. (d) UV–vis–NIR spectra of 130 nm-thick MoO_3/C_{60} composite films measured after thermal annealing at 200 °C (orange), 250 °C (green), and 300 °C (blue) for 1 h in the UHV chamber.

Finally, we examined the thermal stability of the $C_{60}/(MoO_3)_n$ composite film for the practical use of p-type C60-based thermoelectric devices. Figure 4(d) shows the *ex situ* UV–vis–NIR spectra of the composite film before (red) and after thermal annealing at T_a = 200 °C (orange), T_a = 250 °C (green), and T_a = 300 °C (blue) for 1 h under UHV conditions. It is noted that the spectral feature of the composite film remained unchanged even after annealing at 250 °C, indicating that the C_{60}–$(MoO_3)_n$ interactions are thermally stable without structural changes up to 250 °C. However, the intensity of peak 2 tends to increase again after annealing at 300 °C [blue curve in Fig. 4(d)], which suggests the thermal decomposition of $C_{60}/(MoO_3)_n$ complexes.

IV. SUMMARY

We investigated the interactions between C_{60} and $(MoO_3)_n$ using *in situ* STM/STS and *ex situ* UV–vis–NIR spectroscopy in combination with DFT calculations. The formation of $(MoO_3)_n$ chemically bound to C_{60} is energetically favorable due to $\Delta G < 0$ for n = 1, 2, 4, 6, 8, and 9, and they well reproduced the histogram of the $(MoO_3)_n$ height on the C_{60} (111) terrace obtained by the STM height-profile. STS results demonstrated the upward energy shift of both HOMO and LUMO of C_{60} in the vicinity of $(MoO_3)_n$ (n = 6 or 9), which is consistent with the previous results of the co-deposited C_{60}/MoO_3 film obtained using photoemission and inverse photoemission spectroscopy [Refs. 19, 20, and 37]. Theoretical calculations of $(MoO_3)_n$ (n = 1, 2, 4, 6, 8, and 9) chemically bound to C_{60} indicated that 0.01–0.32 holes are injected into C_{60} by $(MoO_3)_n$ nanoclusters, and UV–vis–NIR and DFT results found that the hole doping to C_{60} is caused via the electron transfer from the HOMO of C_{60} to the LUMO of $(MoO_3)_n$. Furthermore, it is noted that the C_{60}–$(MoO_3)_n$ interactions exhibit a high heat resistance up to 250 °C. The present findings provide useful information for the practical use of P-type C_{60}-based thermoelectric devices.

SUPPLEMENTARY MATERIAL

The supplementary material contains Figs. S1–S5 along with their captions.

ACKNOWLEDGMENTS

The present work was financially supported partly by the research collaboration with J-Power Co. Ltd.

AUTHOR DECLARATIONS

Conflict of Interest

The authors have no conflicts to disclose.

Author Contributions

Masato Nakaya: Conceptualization (equal); Data curation (lead); Formal analysis (lead); Investigation (equal); Validation (lead); Visualization (lead); Writing – original draft (lead). **Takuya Kawai**: Data curation (equal); Formal analysis (equal). **Shinta Watanabe**: Data curation (equal); Formal analysis (equal); Investigation (equal). **Jun Onoe**: Conceptualization (equal); Funding acquisition (lead); Investigation (equal); Project administration (lead); Writing – review & editing (lead).

DATA AVAILABILITY

The data that support the findings of this study are available from the corresponding author upon reasonable request.

REFERENCES

[1] H. W. Kroto, J. R. Heath, S. C. O'Brien, R. F. Curl, and R. E. Smalley, Nature **318**, 162 (1985).
[2] M. S. Dresselhaus, G. Dresselhaus, and P. C. Eklund, *Science of Fullerenes and Carbon Nanotubes* (Academic Press, New York, 1995).
[3] *Fullerenes: Chemistry, Physics, and Technology*, edited by K. M. Kadish and R. S. Ruoff (John Wiley & Sons, USA, 2000).
[4] H. Kojima, R. Abe, M. Ito, Y. Tomatsu, F. Fujiwara, R. Matsubara, N. Yoshimoto, and M. Nakamura, Appl. Phys. Exp. **8**, 121301 (2015).
[5] R. C. Yu, N. Tea, M. B. Salamon, D. Lorents, and R. Malhotra, Phys. Rev. Lett. **68**, 2050 (1992).
[6] M.-K. Han, Y. Jin, D.-H. Lee, and S.-J. Kim, Materials **10**, 1235 (2017).
[7] M. Nakaya, S. Watanabe, and J. Onoe, Carbon **152**, 882 (2019).
[8] M. Culter and N. F. Mott, Phys. Rev. **181**, 1336 (1969).
[9] F. Stepniak, P. J. Benning, D. M. Poirier, and J. H. Weaver, Phys. Rev. B **48**, 1899 (1993).
[10] T. Menke, D. Ray, J. Meiss, K. Leo, and M. Riede, Appl. Phys. Lett. **100**, 093304 (2012).
[11] T. Izumi, M. Nakaya, and J. Onoe, Chem. Phys. Lett. **801**, 139744 (2022).
[12] J. Suh, K. M. Yu, D. Fu, X. Liu, F. Yang, J. Fan, D. J. Smith, Y. H. Zhang, J. K. Furdyna, C. Dames, W. Walukiewicz, and J. Wu, Adv. Mater. **27**, 3681 (2015).
[13] S. Kong, T. Wu, M. Yuan, Z. Huang, Q.-L. Meng, Q. Jiang, W. Zhuang, P. Jiang, and X. Bao, J. Mater. Chem. A **5**, 2004 (2017).
[14] C. Falkenberg, C. Uhrich, S. Olthof, B. Maennig, M. K. Riede, and K. Leo, J. Appl. Phys. **104**, 034506 (2008).
[15] M. Kubo, K. Iketaki, T. Kaji, and M. Hiramoto, Appl. Phys. Lett. **98**, 073311 (2011).
[16] M. C. Gwinner, R. D. Pietro, Y. Vaynzof, K. J. Greenberg, P. K. H. Ho, R. H. Friend, and H. Sirringhaus, Adv. Funct. Mater. **21**, 1432 (2011).
[17] T. H. Lee, B. Lüssem, K. Kim, G. Giri, Y. Nishi, and Z. Bao, ACS Appl. Mater. Interfaces **5**, 2337 (2013).
[18] Y. Shinmura, T. Yoshioka, T. Kaji, and M. Hiramoto, Appl. Phys. Express **7**, 071601 (2014).
[19] C. Wang and Y. Gao, Appl. Phys. Lett. **105**, 111601 (2014).
[20] J.-P. Yang, W.-Q. Wang, L.-W. Cheng, Y.-Q. Li, J.-X. Tang, S. Kera, N. Ueno, and X.-h. Zeng, J. Phys.: Condens. Matter **28**, 185502 (2016).
[21] J. Berkowitz and M. G. Inghram, J. Chem. Phys. **26**, 842 (1957).
[22] T. Nakayama, J. Onoe, K. Takeuchi, and M. Aono, Phys. Rev. B **59**, 12627 (1999).
[23] I. Horcas, R. Fernández, J. M. Gómez-Rodríguez, J. Colchero, J. Gómez-Herrero, and A. M. Baro, Rev. Sci. Instrum. **78**, 013705 (2007).
[24] M. J. Frisch, G. W. Trucks, H. B. Schlegel, G. E. Scuseria, M. A. Robb, J. R. Cheeseman, G. Scalmani, V. Barone, G. A. Petersson, H. Nakatsuji, X. Li, M. Caricato, A. Marenich, J. Bloino, B. G. Janesko, R. Gomperts, B. Mennucci, H. P. Hratchian, J. V. Ortiz, A. F. Izmaylov, J. L. Sonnenberg, D. Williams-Young, F. Ding, F. Lipparini, F. Egidi, J. Goings, B. Peng, A. Petrone, T. Henderson, D. Ranasinghe, V. G. Zakrzewski, J. Gao, N. Rega, G. Zheng, W. Liang, M. Hada, M. Ehara, K. Toyota, R. Fukuda, J. Hasegawa, M. Ishida, T. Nakajima, Y. Honda, O. Kitao, H. Nakai, T. Vreven, K. Throssell, J. A. Montgomery, Jr., J. E. Peralta, F. Ogliaro, M. Bearpark, J. J. Heyd, E. Brothers, K. N. Kudin, V. N. Staroverov, T. Keith, R. Kobayashi, J. Normand, K. Raghavachari, A. Rendell, J. C. Burant, S. S. Iyengar, J. Tomasi, M. Cossi, J. M. Millam, M. Klene, C. Adamo, R. Cammi, J. W. Ochterski, R. L. Martin, K. Morokuma, O. Farkas, J. B. Foresman, and D. J. Fox, Gaussian 09, Revision D.01, Gaussian, Inc., Wallingford CT, 2013.
[25] P. Hohenberg and W. Kohn, Phys. Rev. **136**, B864 (1964).
[26] W. Kohn and L. J. Sham, Phys. Rev. **140**, A1133 (1965).
[27] F. Weigend and R. Ahlrichs, Phys. Chem. Chem. Phys. **7**, 3297 (2005).
[28] T. Yanai, D. P. Tew, and N. C. Handy, Chem. Phys. Lett. **393**, 51 (2004).
[29] D. Andrae, U. Häußermann, M. Dolg, H. Stoll, and H. Preuß, Theor. Chem. Acta. **77**, 123 (1990).
[30] B. P. Pritchard, D. Altarawy, B. Didier, T. D. Gibson, and T. L. Windus, J. Chem. Inf. Model. **59**, 4814 (2019).
[31] S. Grimme, J. Antony, S. Ehrlich, and H. Krieg, J. Chem. Phys. **132**, 154104 (2010).
[32] H. L. Schmider and A. D. Becke, J. Mol. Struct.: THEOCHEM **527**, 51 (2000).
[33] T. Lu and F. Chen, J. Comput. Chem. **33**, 580 (2012).
[34] E. Runge and E. K. U. Gross, Phys. Rev. Lett. **52**, 997 (1984).
[35] J. P. Foster and F. Weinhold, J. Am. Chem. Soc. **102**, 7211 (1980).
[36] P. W. Stephens, L. Mihaly, P. L. Lee, R. L. Whetten, S.-M. Huang, R. Kaner, F. Deiderich, and K. Holczer, Nature **351**, 632 (1991).
[37] Z. Li, Z. Fang, M. S. Kelley, B. D. Kay, R. Rousseau, Z. Dohnalek, and D. A. Dixon, J. Phys. Chem. C **118**, 4869 (2014).
[38] N. Doudin, G. Collinge, P. K. Gurunathan, M.-S. Lee, V.-A. Glezakou, R. Rousseau, and Z. Dohnálek, Proc. Natl. Acad. Sci. U. S. A. **118**, e2017703118 (2021).
[39] M. Kröger, S. Hamwi, J. Meyer, T. Riedl, W. Kowalsky, and A. Kahn, Org. Electron. **10**, 932 (2009).
[40] R. J. Hamers, R. M. Tromp, and J. E. Demuth, Phys. Rev. Lett. **56**, 1972 (1986).
[41] C. Domke, P. Ebert, M. Heinrich, and K. Urban, Phys. Rev. B **54**, 10288 (1996).
[42] M. Nishizawa, L. Bolotov, T. Tada, and T. Kanayama, J. Vac. Sci. Technol. B **24**, 365 (2006).
[43] V. I. Srdanov, C. H. Lee, and N. S. Sariciftci, Thin Solid Films **257**, 233 (1995).
[44] Y. Wang, J. M. Holden, A. M. Rao, P. C. Eklund, U. D. Venkateswaran, D. Eastwood, R. L. Lidberg, G. Dresselhaus, and M. S. Dresselhaus, Phys. Rev. B **51**, 4547 (1995).
[45] S. Kazaoui, R. Ross, and N. Minami, Phys. Rev. B **52**, R11665 (1995).